Engineering Structures 266 (2022) 114570

Contents lists available at ScienceDirect

Engineering Structures

journal homepage: www.elsevier.com/locate/engstruct

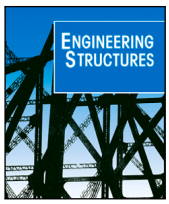

Bayesian updating of tall timber building model using modal data

Blaž Kurent [a], Noemi Friedman [b], Wai Kei Ao [c], Boštjan Brank [a,*]

[a] Faculty of Civil and Geodetic Engineering, University of Ljubljana, Ljubljana, Slovenia
[b] Informatics Laboratory, Institute for Computer Science and Control (SZTAKI), Hungary
[c] College of Engineering, Mathematics and Physical Sciences, University of Exeter, Exeter, UK

ARTICLE INFO

Keywords:
Bayesian model updating
Tall CLT building
Polynomial Chaos surrogate
Uncertainty quantification
Mode pairing
Modal data

ABSTRACT

A framework for the probabilistic finite element model updating based on measured modal data is presented. The described framework is applied to a seven-storey building made of cross-laminated timber panels. The experimental estimates based on the forced vibration test are used in the process of model updating. First, a generalized Polynomial Chaos surrogate model is derived representing the map from the model parameters to the eigenfrequencies and the eigenvectors. To overcome the difficulties caused by mode switching, we propose a novel approach to mode tracking based on partitioning an extended and low-rank representation of the k mode shapes resulting from different setups of the finite element model into k clusters by the k-means clustering algorithm. Second, the surrogate model derived with the help of mode pairing is used to efficiently perform sensitivity analysis and uncertainty quantification of the first five frequencies and the corresponding mode shapes. Finally, the surrogate-based Bayesian update of the model parameters is efficiently performed, providing engineers not only with a finite element model that gives a good fit to the experimental modal data, but also a stochastic model that represents the uncertainties originating from the initial model and the uncertainties of measuring modal properties.

1. Introduction

It has been demonstrated many times (even with the sudden collapse of bridges) that a lot about the actual performance of constructed civil engineering systems (e.g. tall buildings or bridges) under service loading remains unknown. It is extremely difficult to predict a priori the actual performance of a constructed civil engineering system. However, one can perform structural identification in order to narrow the gap between the real system and its numerical model [1]. Structural identification is the process of creating and updating a model of a constructed system based on its measured response. Its basic ingredient is model updating (e.g. [2,3]), which can be performed with either a deterministic or a probabilistic approach.

The deterministic finite element (FE) model updating is well-established, and there have been a number of successful applications in civil engineering systems, see e.g. [4,5] among others. The idea is to parametrize the FE model and use an optimization procedure to update (i.e. calibrate) the model parameters so that the numerical results match the measurements best. The selection of the updating parameters is a key issue in the process, because they have to be directly related to the quantity of interest that is being measured. For civil engineering systems, it is very common that the measurements are designed to estimate modal data (i.e. natural frequencies, mode shapes, and damping ratios for a certain number of vibration modes). However, the modal data identified from the measurements are sensitive to the source and level of excitation, measurement errors, and environmental conditions occurring during the tests. On the other hand, the FE models of civil engineering systems contain unavoidable errors due to idealization, simplification and discretization, as well as uncertainties associated with geometry, material, boundary conditions, and connection details between different elements of the system.

The more informative probabilistic approach to the model updating based on the Bayesian inversion accounts for these errors and uncertainties, see e.g. [6–11]. While with a classical optimization approach we may only find a local minimum point of the chosen cost function, with the probabilistic approach we can recover the posterior distribution of the model parameters given the measured modal properties. In the Bayesian FE model updating, the model parameters are considered as uncertain. They are represented as random variables and described by their posterior marginal distributions, obtained from prior information and measured quantities of interest that depend on the model parameters. The deviation between the measured quantities of interest (i.e. natural frequencies and mode shapes) and the output of the undamped FE modal analysis should be a realization of a random vector predefined as an error model resulting from measurement errors,

* Corresponding author.
E-mail address: bbrank@fgg.uni-lj.si (B. Brank).

https://doi.org/10.1016/j.engstruct.2022.114570
Received 7 January 2022; Received in revised form 11 April 2022; Accepted 16 June 2022
Available online 30 June 2022

from the estimation of modal properties and from the modelling error of the FE model. An improvement in computation time can be achieved by using a surrogate model that approximates the solution of the FE model analysis.

The modal data of a constructed civil engineering system can be obtained from either output-only ambient vibration testing (AVT) or input–output forced vibration testing. The AVT methods are based on measured response due to unmeasured ambient excitations. In the input–output testing, both the excitation force and the corresponding dynamic response are measured, allowing estimation of the frequency response functions (FRFs). The AVT-based estimated modal properties are less reliable than their FRF-based counterparts, [12], yet FRFs have very rarely been used for constructed civil engineering systems. One of the reasons is practical difficulties related to forced excitation of a building or a bridge during its operation. Another reason is a logistical complication in measuring responses simultaneously throughout the structure (which can be solved by using synchronized wireless accelerometers [12]).

For civil engineering systems, there are several works related to the application of Bayesian FE model updating based on modal data, see e.g. [13–17]. In such a process, it is essential that mode pairing is done correctly. The comparison of numerical and measured modal characteristics should be performed only if they correspond to the same eigenmode. In other words, it is essential to determine which FE mode matches which measured mode. This is not an easy task, because only a limited number of degrees of freedom of the mode shapes are being measured. Also, when varying the FE model parameters within the confidence interval, the order of the computed mode shapes may change as well, which calls for a procedure capable of recognizing these changes and correctly linking the FE modes to the corresponding experimental ones. For this purpose, one can use the Modal Assurance Criterion (MAC), see e.g. [13,17]. However, when dealing with spatial aliasing of the experimental mode shapes (when sensors placement does not allow for a clear distinguishing between the experimental modes, e.g. [18,19]), the use of MAC fails and one has to search for another suitable procedure (as is the case in this work).

The applications of modal-data-based Bayesian FE model updating differ in how the error function (and the corresponding likelihood function) is determined for the mode shapes. In some cases, the error of the ith mode shape vector can be effectively defined by means of the corresponding MAC_i value (see e.g. [13,17]). In this work, we not only use the correlation of the experimental mode shapes and the FE modes as a regularization term expressed by the MAC value, but we rather do the update in such a way that we try to fit both the eigenfrequencies and the eigenmodes. By defining an error term expressing our confidence in the measured frequencies and mode shapes, we weigh the importance of accurately fitting the different elements of the different modal properties. Let us also mention that there are updating procedures which do not require matching of experimental and numerical mode shapes, see e.g. [20,21], however, they demand a large number of model parameters.

In this work, we perform the probabilistic FE model updating of a tall timber building (TTB), which is located in Glasgow, UK, and is made completely of cross-laminated timber (CLT) panels. The design of TTBs is governed by the vibration serviceability limit state for the wind-generated vibrations that cause discomfort or annoyance to occupants. Current knowledge on the stiffness and damping of constructed TTBs is limited, particularly with respect to the different types of connections used in different timber load-bearing systems [22,23]. As a result, the understanding of the dynamic behaviour of constructed TTBs under wind-induced vibrations is poor, leading to a lack of confidence by designers to use timber as construction material for new tall buildings. In order to obtain more information about the performance of constructed TTBs under service loadings, a few studies have been performed, see [24–27], some of them including deterministic FE model updating. These and other studies on FE model updating of TTBs are very valuable because they provide insight on how different components of a TTB affect the overall stiffness of the building. Moreover, they provide insight into the as-built stiffness of different structural components in TTBs, in particular shear walls and floors in tall CLT buildings. Namely, in tall CLT buildings, the stiffness is not merely related to the properties of the CLT panels but is also affected (in an unpredictable way) by the joints between the CLT panels, which are essentially steel connections. To the best of our knowledge, the probabilistic FE model updating of TTB (in particular CLT building) is performed for the first time in this work. Another novelty of the presented work is a new procedure for pairing numerical and experimental mode shapes, which is an essential ingredient of the FE model updating based on modal data. It is proposed to use a clustering method to keep track how the order of mode shapes changes with the change of the values of the model parameters. In particular, the k-means clustering method [28] (an unsupervised machine learning algorithm) of an extended, low-rank representation of the mode shapes is applied. The new procedure was designed, because the standard one, which relies on the application of MAC, failed to correctly link the FE mode shapes to the corresponding experimental ones.

With the help of the mode tracking algorithm, a generalized Polynomial Chaos expansion [29] of the natural frequencies and the mode shapes can be computed allowing an efficient evaluation of the modal properties for a given value of the model parameters. The Polynomial Chaos expansion was first introduced by Norbert Wiener [30] to describe stochastic processes with Gaussian random variables with the help of Hermite polynomials. The description was generalized by Xiu [31] to variables with other distributions in the form of what is called generalized Polynomial Chaos (gPC) expansion.

Replacement of the computationally expensive FE modal analysis with the gPC surrogate models allows for efficient computation of the Bayesian inversion by the Markov Chain Monte Carlo (MCMC) sampling method [32]. The surrogate model also allows for fast computation of global sensitivities [33] and statistics of modal properties [31]. The experimental modal data used for model updating were obtained from the input–output testing, where both the excitation force and the corresponding dynamic response were measured, see [12]. FRF-based modal identification was applied to get experimental estimates of the modal properties of the considered tall CLT building. The Bayesian FE model updating of the considered tall CLT building yielded some interesting results. It allowed for an estimation of the as-built stiffness of shear walls and floors, showing the qualitative influence of connections on their stiffness. Moreover, it allows for a statistical evaluation of the quantities of interest, i.e. natural frequencies as well as the mode shapes.

The remainder of the paper is organized in the following way. Section 2 describes the theoretical framework of the applied probabilistic approach. In Section 3, the framework is applied to a seven-storey tall CLT building, and the results of the adopted probabilistic procedure are presented and discussed. In Section 4, the conclusions are drawn.

2. Probabilistic framework

Let $\mathbf{p} \in \mathbb{R}^N$ be a vector of chosen uncertain input parameters of the FE model. In the Bayesian framework, we model these parameters as random variables denoted by $\mathbf{P}: \Omega \to \mathbb{R}^N$, with Ω being the set of all possible outcomes. We denote the vector of random variables with a capital letter and a certain realization of it with a small letter.[1] Our uncertainty of the 'true' values of the chosen parameters is reflected by the variance of the random variables. The prior uncertainty should reflect our prior knowledge about what values the parameters

[1] E.g. $\boldsymbol{\Xi}$ denotes the random variable and $\boldsymbol{\xi}$ denotes a realization of the random variable $\boldsymbol{\Xi}$.

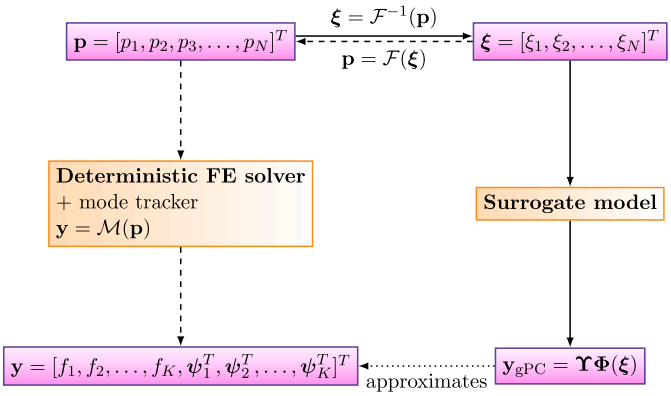

Fig. 1. Replacing the deterministic FE solver by a PCE surrogate model: the dashed line shows the path without a surrogate model and the solid line shows the one when a surrogate model is used.

can take with what probabilities. This is often based on experiments, professional expertise and engineering judgement.

Let $\pi_{\mathbf{P}}(\mathbf{p})$ be the joint probability distribution of the random vector $\mathbf{P}$. When the uncertain parameters P_i are mutually independent random variables, this distribution is the product of the univariate distributions

$$\pi_{\mathbf{P}}(\mathbf{p}) = \prod_{i=1}^{N} \pi_{P_i}(p_i). \tag{1}$$

Let us denote in an abstract way the operation of getting the measurable outputs $\mathbf{y}$ from a specific realization of the parameters $\mathbf{p}$ with the forward operator $\mathcal{M} : \mathbb{R}^N \to \mathbb{R}^L$

$$\mathbf{y} = \mathcal{M}(\mathbf{p}), \quad \mathbf{y} \in \mathbb{R}^L. \tag{2}$$

We use measurements of modal features to calibrate the FE model. To this end, we define a measurable quantity

$$\mathbf{y} = \left[f_1, \quad f_2, \quad \ldots, \quad f_K, \quad \boldsymbol{\psi}_1^T, \quad \boldsymbol{\psi}_2^T, \quad \ldots, \quad \boldsymbol{\psi}_K^T\right]^T, \tag{3}$$

where $f_i \in \mathbb{R}$ and $\boldsymbol{\psi}_i \in \mathbb{R}^D$ are the ith eigenfrequency and eigenvector, respectively. D is the number of measured degrees of freedom (dimension of the eigenvector) and K is the number of the modes used in the update procedure. These two constants give the dimension of the measured quantity $L = (1 + D)K$. The measured counterpart $\mathbf{z}_{\mathrm{meas}}$ is linked to the 'true' value of the input variables $\mathbf{p}_{\mathrm{meas}}$ as

$$\mathbf{z}_{\mathrm{meas}} = \mathcal{M}(\mathbf{p}_{\mathrm{meas}}) + \boldsymbol{\epsilon}, \tag{4}$$

where $\boldsymbol{\epsilon}$ is one realization of the vector of random variables $\mathbf{E} : \Omega \to \mathbb{R}^L$ representing the sum of the modelling error and the measurement noise. We denote the probability density of the error model $\mathbf{E}$ by π_E.

2.1. Bayesian inversion

With a probabilistic identification, we wish to express the conditional distribution of the input random variables given a specific measured value $\mathbf{z}_{\mathrm{meas}}$ of the measurable quantity $\mathbf{y}$. The updated, posterior distribution of the parameters according to Bayes' theorem is

$$\underbrace{\pi_{\mathbf{P}|\mathbf{z}_{\mathrm{meas}}}(\mathbf{p})}_{\text{posterior}} = \frac{\overbrace{\pi_{\mathbf{z}_{\mathrm{meas}}|\mathbf{P}}(\mathbf{p})}^{\text{likelihood}}\overbrace{\pi_{\mathbf{P}}(\mathbf{p})}^{\text{prior}}}{\underbrace{\int_{I_{\mathbf{P}}} \pi_{\mathbf{z}_{\mathrm{meas}}|\mathbf{P}}(\mathbf{p})\pi_{\mathbf{P}}(\mathbf{p})d\mathbf{p}}_{\text{evidence}}} = \frac{\mathcal{L}(\mathbf{p})\pi_{\mathbf{P}}(\mathbf{p})}{\zeta}, \tag{5}$$

where the numerator is the product of the likelihood and the prior and the denominator, the evidence is just the normalization factor assuring that the density function integrates to one. The likelihood $\mathcal{L}(\mathbf{p}) = \pi_{\mathbf{z}_{\mathrm{meas}}|\mathbf{P}}(\mathbf{p})$ of measuring a specific value of measurable quantity $\mathbf{z}_{\mathrm{meas}}$ given a certain value of parameter $\mathbf{p}$ can be computed from the determination of the probability that the measurement error takes the value $\boldsymbol{\epsilon} = \mathbf{z}_{\mathrm{meas}} - \mathbf{y}$, i.e.,

$$\mathcal{L}(\mathbf{p}) = \pi_{\mathbf{E}}\left(\mathbf{z}_{\mathrm{meas}} - \mathcal{M}(\mathbf{p})\right). \tag{6}$$

The prior distribution can strongly influence the posterior distribution and should therefore be carefully chosen based on engineering judgement (see more on the potential influence of prior distribution on the posterior in [11]).

Unfortunately, it would be difficult to write the posterior distribution in a closed form. Therefore, we rather sample from the given distribution using the Metropolis–Hastings algorithm [32,34]. The basic idea of the algorithm is to generate samples by a random walk in the parameter space, such that the stationary distribution of this process equals the target distribution (in this case the Bayes posterior). That is, after an initial transient phase (burn-in period) sampling from the random walk is equivalent to directly sampling from the posterior. The random walk is governed by what is called proposal density. According to this conditional distribution, a new point of random walk is proposed, depending on the current point of the walk. The proposed point is then accepted at each step of the walk with a probability of the ratio between posterior in the new proposed point and posterior in the current point. Otherwise, it is rejected and a new point is proposed for the next step from the current point. The algorithm that uses a surrogate model is explained in detail in [35].

The Metropolis–Hastings algorithm has the advantage that we can ignore the computation of the normalization factor, the evidence, and that, unlike some sampling-free methods, it does not impose any requirements on the posterior distribution (e.g. to be Gaussian). Nevertheless, with such a sampling method a large number of evaluations of the likelihood is needed. For one evaluation of the likelihood the measurable quantity $\mathbf{y} = \mathcal{M}(\mathbf{p})$ (in our example here the frequencies and the mode shapes) have to be computed from a specific value of the input parameters. As we need a large number of evaluations, it is often unaffordable to call the FE solver for each evaluation. In order to avoid this cost and also for efficient sensitivity analysis and computation of statistics, we first replace the FE model with a surrogate model, a gPC expansion $\mathbf{y}_{\mathrm{gPC}} = \mathcal{M}_{\mathrm{gPC}}(\mathbf{p})$ which approximates the modal properties $\mathbf{y}$ in the form of multivariate polynomials of the input parameters $\mathbf{p}$, as is schematically presented in Fig. 1. The random walk using a surrogate model is explained in detail in [35]. For computational convenience, instead of directly using the random variables of the input parameter for the expansion, we map them to some reference random variables

$$\boldsymbol{\Xi} = [\Xi_1, \Xi_2, \ldots, \Xi_N]^T, \tag{7}$$

the components of which are mutually independent random variables with some standard distribution. The map from the reference parameter to the input parameter is denoted here by

$$\mathbf{p} = \mathcal{F}(\boldsymbol{\xi}). \tag{8}$$

The gPC expansion takes the form

$$\mathbf{y} = \mathcal{M}(\mathbf{p}) \approx \mathcal{M}_{\mathrm{gPC}}(\mathbf{p}) = \mathbf{y}_{\mathrm{gPC}}\underbrace{(\mathcal{F}^{-1}(\mathbf{p}))}_{\boldsymbol{\xi}} = \sum_{m=1}^{M} \boldsymbol{\upsilon}_m \Phi_m(\boldsymbol{\xi}) = \boldsymbol{\Upsilon}\boldsymbol{\Phi}(\boldsymbol{\xi}), \tag{9}$$

where Φ_m are the orthogonal multivariate polynomials and $\boldsymbol{\upsilon}_m \in \mathbb{R}^L$ are the coefficients of the expansion corresponding to the mth polynomial, $\boldsymbol{\Phi} \in \mathbb{R}^M$ is a vector collecting all the polynomials and $\boldsymbol{\Upsilon} \in \mathbb{R}^{L\times M}$ a matrix collecting the vectors of coefficients $\boldsymbol{\upsilon}_m$ in its columns. With the help of the expansion, the likelihood can be approximated by

$$\mathcal{L}(\mathbf{p}) \approx \pi_E(\mathbf{z}_{\mathrm{meas}} - \mathcal{M}_{\mathrm{gPC}}(\mathbf{p})). \tag{10}$$

With the given framework we can sample from the posterior distribution and make a point estimate of the input parameters by estimating the maximum a-posteriori (MAP) point – the mode of the samples – or the mean of the posterior distribution.

2.2. Generalized polynomial chaos expansion

The main idea of computing a surrogate model is to approximate the dependence of the measurable variables $\mathbf{y}$ on the reference variables $\boldsymbol{\xi}$ with the help of a set of M polynomial basis functions $\{\boldsymbol{\Phi}_m\}_{m=1}^{M}$ that are orthogonal with respect to the underlying probability space, that is

$$\mathbb{E}[\boldsymbol{\Phi}_m(\boldsymbol{\xi})\boldsymbol{\Phi}_n(\boldsymbol{\xi})] = \int_{\mathbb{R}^N} \boldsymbol{\Phi}_m(\boldsymbol{\xi})\boldsymbol{\Phi}_n(\boldsymbol{\xi})\pi_{\boldsymbol{\Xi}}(\boldsymbol{\xi})\mathrm{d}\boldsymbol{\xi} = \gamma_m\delta_{mn}, \tag{11}$$

where $\pi_{\boldsymbol{\Xi}}(\boldsymbol{\xi})$ is the joint probability distribution of the reference random variables $\boldsymbol{\Xi}$, δ_{mn} is the Kronecker delta, and γ_m is the squared norm of the polynomials, that is

$$\gamma_m = \mathbb{E}[\boldsymbol{\Phi}_m(\boldsymbol{\xi})\boldsymbol{\Phi}_m(\boldsymbol{\xi})] = \int_{\mathbb{R}^N} \boldsymbol{\Phi}_m(\boldsymbol{\xi})\boldsymbol{\Phi}_m(\boldsymbol{\xi})\pi_{\boldsymbol{\Xi}}(\boldsymbol{\xi})\mathrm{d}\boldsymbol{\xi}. \tag{12}$$

The type of polynomials used for the expansion depends on the distributions of the reference random variables Ξ_i. For example, when all the reference parameters have a standard Gaussian distribution, the polynomials that are orthogonal with respect to this probability measure are the Hermite polynomials. With the help of the orthogonal polynomials, the measurable modal properties $\mathbf{y}$ can be written as a linear combination of these polynomials $\boldsymbol{\Phi}_m$ with coefficients $\boldsymbol{\upsilon}_m$,

$$\begin{aligned}\mathbf{y} &= \mathcal{M}(\mathbf{p}) = \mathcal{M}(\mathcal{F}(\boldsymbol{\xi})) \approx \mathcal{M}_{\mathrm{gPC}}(\mathbf{p}) = \mathbf{y}_{\mathrm{gPC}}(\mathcal{F}^{-1}(p)) \\ &= \sum_{m=1}^{M} \boldsymbol{\upsilon}_m\boldsymbol{\Phi}_m(\boldsymbol{\xi}) = \boldsymbol{\Upsilon}\boldsymbol{\Phi}(\boldsymbol{\xi}).\end{aligned} \tag{13}$$

The gPC coefficients $\boldsymbol{\upsilon}_m$ can be computed by different techniques, e.g. interpolation, orthogonal projection, regression (see e.g. [29]). Here, we only describe how to compute the coefficients by regression. First, we write the error of the approximation at a sample point $\boldsymbol{\xi}_j$ of the reference random variables

$$\mathbf{e}(\boldsymbol{\xi}_j) = \mathbf{y}(\boldsymbol{\xi}_j) - \mathbf{y}_{\mathrm{gPC}}(\boldsymbol{\xi}_j) = \mathbf{y}(\boldsymbol{\xi}_j) - \sum_{m=1}^{M} \boldsymbol{\upsilon}_m\boldsymbol{\Phi}_m(\boldsymbol{\xi}_j), \tag{14}$$

and we compute the coefficients by requiring the mean squared error of the approximation for all components l at some chosen sample points $\{\boldsymbol{\xi}_j\}_{j=1}^{Q}$

$$s_l = \sum_{j=1}^{Q}([\mathbf{e}(\boldsymbol{\xi}_j)]_l)^2 \quad l = 1 \dots L \tag{15}$$

to be minimized. The sum s_l reaches its minimum, where the gradient is zero, that is

$$\begin{aligned}\frac{\partial s_l}{\partial[\boldsymbol{\upsilon}_m]_l} &= -2\sum_{j=1}^{Q}[\mathbf{e}(\boldsymbol{\xi}_j)]_l\frac{\partial[\mathbf{y}_{\mathrm{gPC}}]_l}{\partial[\boldsymbol{\upsilon}_m]_l} \\ &= -2\sum_{j=1}^{Q}[\mathbf{e}(\boldsymbol{\xi}_j)]_l\boldsymbol{\Phi}_m(\boldsymbol{\xi}_j) = 0 \quad \forall \quad l = 1 \dots L.\end{aligned} \tag{16}$$

Accordingly, coefficients $\boldsymbol{\Upsilon}$ can be computed by solving the system of equations

$$-2\,(\mathbf{A} - \boldsymbol{\Upsilon}\mathbf{F})\,\mathbf{F}^T = \mathbf{0}, \tag{17}$$

where the elements of matrix $\mathbf{A} \in \mathbb{R}^{L\times Q}$ are the modal properties computed at the different sample points $\boldsymbol{\xi}_j$

$$[\mathbf{A}]_{l,j} = [\mathbf{y}(\boldsymbol{\xi}_j)]_l \tag{18}$$

and the matrix $\mathbf{F} \in \mathbb{R}^{M\times Q}$ is the interpolation matrix, the basis functions evaluated at the sample points

$$[\mathbf{F}]_{m,j} = \boldsymbol{\Phi}_m(\boldsymbol{\xi}_j). \tag{19}$$

2.3. Eigenmode ordering

Even though matrix $\mathbf{A}$ is only a collection of eigenfrequencies and eigenvectors computed at Q different values of the uncertain parameters, it is not straightforward to assemble it. The main difficulty in computing the $\mathbf{y}(\boldsymbol{\xi}_j)$ vectors is caused by the possible mode switching that can occur when the values of the input parameters are deviated. Thus, the main issue when generating the surrogate model is to order the components of vector $\mathbf{y}$ well, see Eq. (3).

The classical approach is to correlate the FE mode shapes with the experimental ones and to use the order of the latter as a ground ordering. This is usually done by the MAC criterion (for more see Section 3.4). However, not only the frequencies but also the mode shapes change with the changing values of the parameters. Due to the change of the shapes, the correlation with the right experimental mode decreases. Together with spatial aliasing where otherwise uncorrelated modes show correlation, it is difficult to match the right mode pair. The ambiguity of MAC matrix for the pairing of the modes can be observed in the case studied in this paper, see Section 3.4.

For the task at hand, to cluster the $Q \times K$ mode shapes into K sets, 1st, 2nd...Kth mode, the k-means unsupervised clustering can be used. The idea is to partition the modes into K sets

$$S = \{S_1, S_2, \dots, S_K\} \tag{20}$$

in such way that each mode shape $\boldsymbol{\psi}_k^j$ belongs to the set with the nearest mean,

$$S = \arg\min_{S} \sum_{k=1}^{K}\sum_{\boldsymbol{\psi}\in S_k} \|\boldsymbol{\psi} - \boldsymbol{\mu}_k\|^2, \tag{21}$$

that is, the sets are chosen such that the summed variances of the mode shapes in between the clusters are minimized. In Eq. (21), $\boldsymbol{\mu}_k$ is the mean of the mode shapes that belong to set S_k. To improve the quality of the clustering, not only the mode shapes but also their derivatives can be included in the clustering procedure. If the original mode shape $\boldsymbol{\psi}$ was a vector of displacements in the x_1 direction and in the x_2 direction

$$\boldsymbol{\psi} = \left[\boldsymbol{\psi}_{x_1}^T, \boldsymbol{\psi}_{x_2}^T\right]^T, \quad \boldsymbol{\psi} \in \mathbb{R}^D \tag{22}$$

the modified vector can be extended by the derivatives of the mode shapes

$$\tilde{\boldsymbol{\psi}} = \left[\boldsymbol{\psi}_{x_1}^T, \boldsymbol{\psi}_{x_2}^T, \left(\frac{\partial\boldsymbol{\psi}_{x_1}}{\partial x_3}\right)^T, \left(\frac{\partial\boldsymbol{\psi}_{x_2}}{\partial x_3}\right)^T\right]^T \quad \tilde{\boldsymbol{\psi}} \in \mathbb{R}^{\tilde{D}}. \tag{23}$$

By extending the vector, the success of the clustering is increased, especially when the number of sensor locations is limited. The k-means clustering method, unfortunately, suffers from the curse of dimensionality. When the dimension of mode shapes $\boldsymbol{\psi}$ is high, the performance of the clustering decreases. To overcome this problem, a low-rank representation can be used with the help of the proper orthogonal decomposition (POD) to compensate for the increased dimension $\tilde{D}$ of the extended mode shape vector $\tilde{\boldsymbol{\psi}}$. If we collect all K extended eigenvectors $\tilde{\boldsymbol{\psi}}_k$ for all the Q sample points in a big matrix $\mathbf{U}$ with $K\cdot Q$ columns, the POD of this $\mathbf{U}$ matrix reads

$$\mathbf{U} = \boldsymbol{\mu}_{\tilde{\boldsymbol{\psi}}} + \tilde{\mathbf{U}} = \boldsymbol{\mu}_{\tilde{\boldsymbol{\psi}}} + \mathbf{VSW} = \boldsymbol{\mu}_{\tilde{\boldsymbol{\psi}}} + \sum_{m=1}^{\tilde{D}} \sigma_m\mathbf{v}_m w_m, \quad \mathbf{U}, \tilde{\mathbf{U}} \in \mathbb{R}^{\tilde{D}\times(K\cdot Q)}, \tag{24}$$

where $\boldsymbol{\mu}_{\tilde{\boldsymbol{\psi}}}$ is a matrix where each column is the mean of all the $K\cdot Q$ extended vectors $\tilde{\boldsymbol{\psi}}$, and $\tilde{\mathbf{U}}$ is the fluctuating part of the columns, $\mathbf{S} \in \mathbb{R}^{\tilde{D}\times\tilde{D}}$ is a diagonal matrix with $[\mathbf{S}]_{mm} = \sigma_m$. The orthogonal matrix $\mathbf{V} \in \mathbb{R}^{\tilde{D}\times\tilde{D}}$ of the decomposition of the fluctuating part can be computed by the eigenvalue decomposition of the covariance matrix $\mathbf{C}$, namely

$$\mathbf{C} = \mathrm{cov}(\mathbf{U}) = \mathbb{E}(\tilde{\mathbf{U}}\tilde{\mathbf{U}}^T) = \mathbf{VS}^2\mathbf{V}^T. \tag{25}$$

The columns of matrix $\mathbf{V}$, vectors $\mathbf{v}_m$, are representative for the description of the mode shapes in the sense that they can best capture

Fig. 2. A photo of Yoker from November 2019.

their variance. The terms with smaller values of σ_m do not significantly contribute to the variance, so they can be ignored in the expansion, leading to a truncated set of basis functions $\{\mathbf{v}_m\}_{m=1}^{D'}$, where $D' < \tilde{D}$. With this ideal set of basis vectors at hand, we cluster the extended mode shape vectors described in the truncated basis, that is, instead of clustering the vectors $\tilde{\boldsymbol{\psi}}$ we cluster the vectors projected onto this reduced dimensional basis

$$\tilde{\boldsymbol{\psi}}_k = \hat{\mathbf{V}}^T \tilde{\boldsymbol{\psi}}, \tag{26}$$

where $\hat{\mathbf{V}} \in \mathbb{R}^{\tilde{D} \times D'}$ is the truncated matrix of basis functions $\{\mathbf{v}_m\}_{m=1}^{D'}$.

Even though all the eigenvectors $\boldsymbol{\psi}$ are normalized, there is still the problem of flipped mode shapes. To tackle this problem, we can cluster the mode shapes into twice as many clusters as there were modes in the group, each cluster having its flipped version.

2.4. Uncertainty quantification and sensitivity analysis

Once the final surrogate model is constructed the evaluation of the statistics and the sensitivities of the modal properties can be efficiently computed. The uncertainty of the outputs is estimated based on the propagation of uncertainties of the input parameters (i.e. prior distributions) through the model.

If we chose the first polynomial to be $\Phi_1 = 1$, the mean of the modal properties $\mathbf{Y}$, for example, can be computed directly from the gPC coefficients corresponding to the zeroth polynomial

$$\begin{aligned}\mathbb{E}[\mathbf{Y}] \approx \mathbb{E}[\mathbf{Y}_{\mathrm{gPC}}] &= \mathbb{E}\left[\sum_m \boldsymbol{\upsilon}_m \Phi_m(\boldsymbol{\Xi})\right] = \sum_m \boldsymbol{\upsilon}_m \mathbb{E}[\Phi_m(\boldsymbol{\Xi})] \\ &= \sum_m \boldsymbol{\upsilon}_m \mathbb{E}[\Phi_m(\boldsymbol{\Xi}) \underbrace{\Phi_1(\boldsymbol{\Xi})}_{=1}] = \boldsymbol{\upsilon}_1,\end{aligned} \tag{27}$$

because of $\mathbb{E}[\Phi_1 \Phi_1] = 1$ and $\mathbb{E}[\Phi_{m\neq 1} \Phi_1] = 0$ due to the orthogonality condition (11). The variance of $\mathbf{Y}$ can be computed from the rest of the coefficients by

$$\begin{aligned}\mathrm{cov}[\mathbf{Y}, \mathbf{Y}] \approx \mathrm{cov}[\mathbf{Y}_{\mathrm{gPC}}, \mathbf{Y}_{\mathrm{gPC}}] &= \mathbb{E}\left[\left(\sum_{m=1}^{M} \boldsymbol{\upsilon}_m \Phi_m(\boldsymbol{\Xi}) - \mathbb{E}[\mathbf{Y}_{\mathrm{gPC}}]\right) \right. \\ &\quad \left. \times \left(\sum_{m=1}^{M} \boldsymbol{\upsilon}_m \Phi_m(\boldsymbol{\Xi}) - \mathbb{E}[\mathbf{Y}_{\mathrm{gPC}}]\right)^T\right] \\ &= \sum_{m=2}^{M} \boldsymbol{\upsilon}_m \boldsymbol{\upsilon}_m^T \gamma_m,\end{aligned} \tag{28}$$

again because of the orthogonality condition (11).

The Sobol indices, the variance-based sensitivity measures, show the ratio of the variance attributable to the uncertainties of a given set of input parameters (or of one parameter in the case of the linear indices) and the total variance. The partial variances can also be directly computed from the coefficients of the gPC expansion [33].

3. Case study: tall CLT building

In this section, the above-presented probabilistic framework is applied for a seven-storey building in Glasgow, UK, called Yoker (see Fig. 2). The application steps are illustrated in Fig. 3. The building and its FE model were already described in [36]. Therefore, only basic information is given hereinafter.

The floor plan of the building is of T-shape, with a "flange" and a "web" connected by a narrow corridor. Apart from a few steel beams and frames that act as local reinforcements, the structure of the building is made entirely of CLT panels with 3 or 5 layers and a thicknesses of 100 mm to 140 mm. Almost all external walls are large (one storey high) CLT panels with pre-cut openings. The majority of internal walls are load-bearing CLT walls. The floor slabs are made of smaller CLT panels connected with wood screws. The walls and the floor slabs are connected by angle brackets and wood screws.

The FE model for computing eigenfrequencies and eigenvectors of Yoker was prepared by Ansys [37]. The study [36] revealed that modelling of the foundation and the soil is not necessary when dynamic response with small vibration amplitudes is studied. For this reason, only the above ground part of the structure was modelled, with degrees of freedom restrained to zero at the bottom of the mesh. A fine mesh (with 2.61×10^5 nodes) consisting of multi-layered shell elements was used, with an orthotropic material model applied at each layer. As for the material properties of the layers, the mean data provided by the manufacturer (StoraEnso) [38] were considered, with the elastic moduli of 12 000 MPa and 370 MPa in major and minor strength directions, respectively, a shear modulus parallel to the fibre direction of 460 MPa, and a density of 470 kg m^{-3} (Poisson's ratio $\nu_{12} = 0.3$ was assumed). Some of the elastic constants were chosen as uncertain parameters, as described in Section 3.1. The joints between the panels were not modelled as special entities, but an ideal bond was assumed. The elements of the building that were considered as entities with stiffness are the external and the internal load-bearing walls, floors, roof and elevator shaft. The neglected building elements include steel beams and frames, non-load-bearing partition walls, stairs and windows. The mass of the timber part of the building, which is estimated at 515 t, was applied through timber density. The mass of well-documented non-structural elements (i.e. facade, insulation, screed, flooring, fireline board, cladding, and non-load-bearing partition walls) that is estimated at 685 t was distributed over the FEs modelling floor slabs and walls. The estimate of the remaining mass (including doors, windows, stairs, live load, etc.) was 70 t, which yielded $q = 25\,\mathrm{kg/m^2}$ when smeared over the FEs modelling floor slabs.

The first five modes calculated by the FE model are presented in Fig. 4. Mode 1 is a bending mode, modes 2 and 3 are torsion modes. Modes 4 and 5 are more complex torsion and shear modes, respectively.

3.1. Uncertain parameters of the FE model

The originally deterministic FE model is transformed into a stochastic one, by treating a chosen set of its input parameters as random variables. In this way, the FE model depends on the actual realization of the value of these parameters. The choice was based on professional expertise and an educated guess established by an extensive one-at-the-time sensitivity analysis, as well as on the conclusions drawn from the deterministic FE model updating of Yoker presented in [36].

The parameters enter the FE model as elastic constants of different segments of the structure, such as elastic moduli in major strength direction (e_1, e_2, e_3) and in-plane shear moduli (g_1, g_2), together with

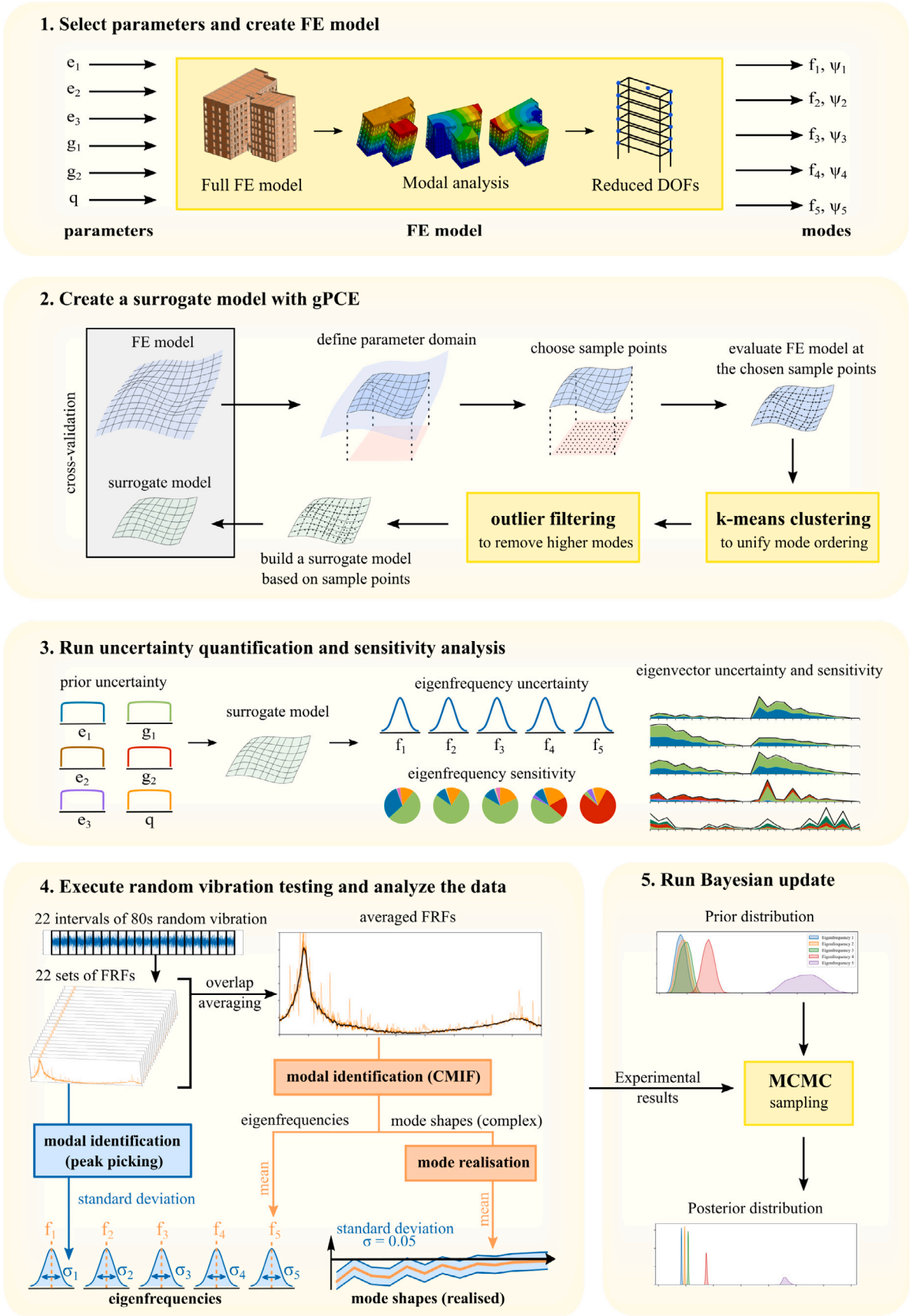

Fig. 3. Application of the proposed concept to Yoker building.

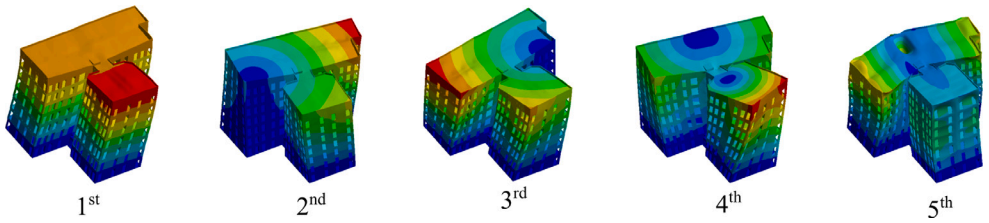

Fig. 4. First five mode shapes of the initial model.

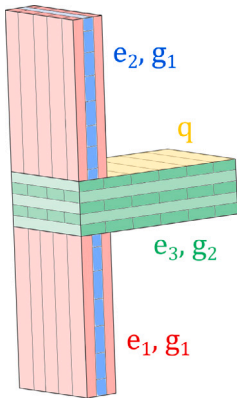

Fig. 5. Six uncertain parameters of the FE model.

Table 1
Chosen parameters and their bounds.

Parameter	Prior distribution	Property	Application
e_1 [GPa]	$\mathcal{U}(6, 12)$	E_1	CLT panels in walls. Only for layers with fibres in vertical direction.
e_2 [GPa]	$\mathcal{U}(10, 13)$	E_1	CLT panels in walls. Only for layers with fibres in horizontal direction.
e_3 [GPa]	$\mathcal{U}(6, 12)$	E_1	CLT panels in floor slabs. All layers.
g_1 [MPa]	$\mathcal{U}(400, 750)$	G_{12}	CLT panels in walls. All layers.
g_2 [MPa]	$\mathcal{U}(200, 500)$	G_{12}	CLT panels in floor slabs. All layers.
q [kg m^{-2}]	$\mathcal{U}(5, 100)$	Mass	Additional distributed mass along all floors.

one distributed mass parameter (q). The assignment of stiffness and mass parameters to the different segments is explained in Table 1 and illustrated in Fig. 5. Although the parameters enter the FE model as material and mass properties, they were selected to capture two types of uncertainties. The first type is related to the stochastic nature of CLT material data and a lack of knowledge about the mass of the building. The second type is related to the influence of the joints (with steel connections) between the CLT panels on the overall stiffness of the building.

The vector of the uncertain parameters is now

$$\mathbf{p} = [e_1, e_2, e_3, g_1, g_2, q]^T, \quad \mathbf{p} \in \mathbb{R}^6. \tag{29}$$

Based on the above-described prior analysis we assigned bounds a_i and b_i to all p_i parameters and we supposed an uninformative prior in between these bounds, i.e. a uniform marginal distribution $P_i \sim \mathcal{U}(a_i, b_i)$ of these parameters. The assigned distributions with their bounds are given in Table 1. Furthermore, we assume that the parameters are independent random variables. The vector of the reference random variables

$$\boldsymbol{\Xi} = [\Xi_1, \Xi_2, \Xi_3, \Xi_4, \Xi_5, \Xi_6]^T, \tag{30}$$

has components with standard uniform distributions, that is, $\Xi_i \sim \mathcal{U}(-1, 1)$. The mapping is given by shifting and scaling the random variables

$$\mathbf{p} = \mathcal{F}(\boldsymbol{\xi}), \quad p_i = \mathcal{F}_i(\xi_i) = s_i \xi_i + m_i, \quad i = 1, \dots, 6, \tag{31}$$

where $s = (b_i - a_i)/2$ and $m_i = \frac{a_i + b_i}{2}$. The joint distribution of the new set of random variables $\boldsymbol{\Xi}$ is

$$\pi_{\boldsymbol{\Xi}}(\boldsymbol{\xi}) = \prod_{i=1}^{6} \pi_{\Xi_i}(\xi_i) = \begin{cases} 0.5^6 & \text{for} \quad \boldsymbol{\xi} \in [-1, 1]^6 \\ 0 & \text{otherwise,} \end{cases} \tag{32}$$

and the joint distribution of the original set of parameters is

$$\pi_{\mathbf{P}}(\mathbf{p}) = \prod_{i=1}^{6} \pi_{P_i}(p_i), \tag{33}$$

where

$$\pi_{P_i}(p_i) = \begin{cases} \frac{1}{b_i - a_i} & \text{for} \quad p_i \in [a_i, b_i] \\ 0 & \text{otherwise.} \end{cases} \tag{34}$$

3.2. Eigenmode ordering and computation of the surrogate model

For the computation of the coefficients of the gPC surrogate model, $Q = 10.000$ quasi-Monte Carlo (QMC) sample points were generated by the Halton sequence drawn from the uniform distribution $\pi_{\boldsymbol{\Xi}}(\boldsymbol{\xi})$.

Each sample point $\boldsymbol{\xi}$ was mapped by Eq. (31) into parameter vector $\mathbf{p}$, which was further used to compute the vector of modal properties $\mathbf{y}$. This is done by forward operator $\mathcal{M}$, which represents in an abstract way the computation of the eigenfrequencies and eigenvectors for a given $\mathbf{p}$ using the FE software

$$\mathbf{y} = \left[f_1, f_2, f_3, f_4, f_5, \boldsymbol{\psi}_1^T, \boldsymbol{\psi}_2^T, \boldsymbol{\psi}_3^T, \boldsymbol{\psi}_4^T, \boldsymbol{\psi}_5^T\right]^T = \mathcal{M}(\mathbf{p}), \quad \mathbf{y} \in \mathbb{R}^L. \tag{35}$$

Each eigenvector $\boldsymbol{\psi}_k$ in (35) is defined by 13 points in the $x_1 - x_2$ plane, as presented in Section 3.4. More precisely, 13 nodes of the mesh that coincide with the 13 sensor locations during the experimental testing are used to construct $\boldsymbol{\psi}_k$,

$$\boldsymbol{\psi}_k^T = \left[\psi_{k,x_1}^1, \dots, \psi_{k,x_1}^{13}, \psi_{k,x_2}^1, \dots, \psi_{k,x_2}^{13}\right], \quad k = 1, \dots, 5. \tag{36}$$

The dimension of $\boldsymbol{\psi}_k$ is $D = 13 \cdot 2 = 26$, and $L = K + K \cdot 13 \cdot 2 = 135$.

Before the results of the computations were applied to assemble matrix $\mathbf{A}$, the eigenvectors were normalized with the Euclidean norm in order to adjust the experimental and the numerical results to the same normalization. An illustration of the procedure used to construct the surrogate model with the inherent mode ordering is given in point 2 of Fig. 3.

When preparing the surrogates for the eigenvectors, we encountered a difficulty with the consistent ordering of the eigenvectors. The usual approach based on MAC resulted in incorrect ordering, as shown in Fig. 6 (left). As natural frequencies greatly overlap (see Fig. 7), they could not be used to determine the right ordering. In addition, there was a problem of flipped eigenvectors that cannot be simply solved with normalization. These issues were approached with the technique of clustering and filtering described in Section 2.3.

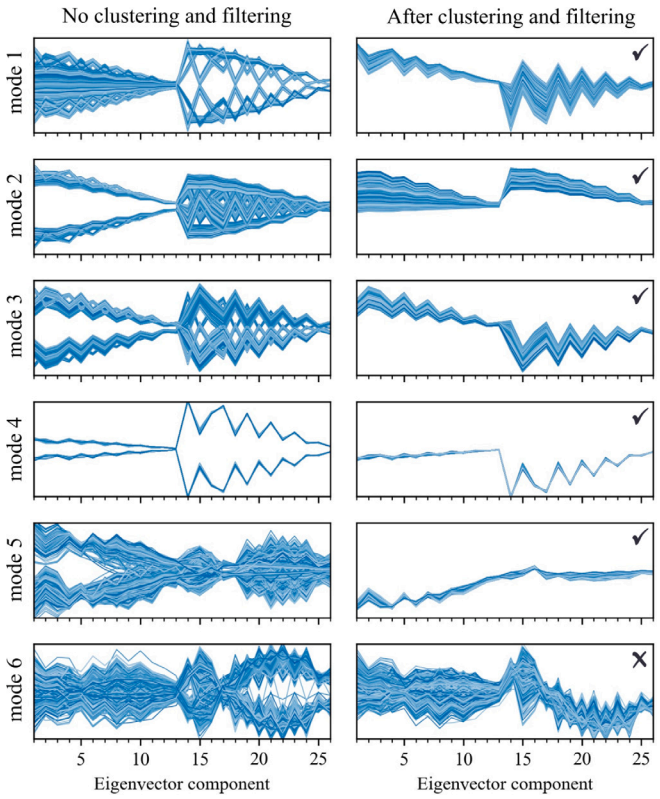

Fig. 6. Normalized eigenvectors with ordering based on the MAC values (left) and after the clustering and filtering (right). On the horizontal axis, there are x_1 and x_2 values at 13 sensor locations.

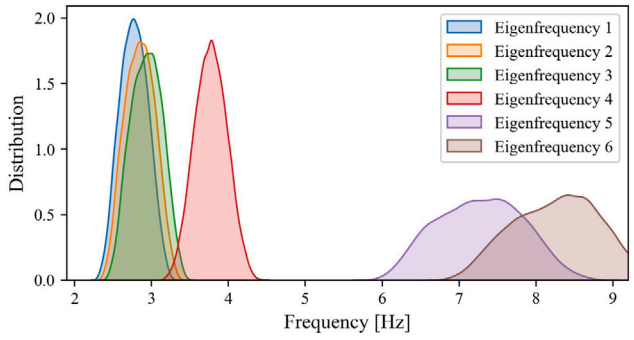

Fig. 7. Distribution of the first six eigenfrequencies before the clustering.

We included six modes in the clustering process to obtain five well-ordered modes. The computed modes were divided into three groups - (i) the first three modes, (ii) the fourth mode and (iii) the fifth and the sixth modes — that were clustered separately. Because the frequencies of the first three modes were very close to each other (see Fig. 7) and distinguishable from mode four, switching of the modes within this three modes is very plausible, but a switch to mode four is not. Figs. 6 and 7 show that mode four is easily separable from the others. Finally, modes five and six were expected to switch between each other (with probable involvement of some higher modes).

As described in Section 2.3, for a better clustering process we worked with an extended vector $\tilde{\boldsymbol{\psi}}_i$. However, for numerical convenience, we did not compute the derivatives, but we extended the vector by the differences in displacements between the subsequent points. This resulted in the extended dimension $\tilde{D} = 26+25 = 51$. To enhance the effectiveness of the approach to cluster the eigenmodes (see Section 2.3), we initiated the mean of the clusters $\boldsymbol{\mu}_{\tilde{\psi}}$ to be the mode shapes computed with the mean values of the prior input parameters, and their flipped versions in the clustering procedure. For further analysis, we flip back the mode shapes belonging to half of the clusters such that the mode shapes have the same sign as the experimental eigenvector. Also following Section 2.3, we used a low-rank representation of the extended eigenvectors. The reduced dimension D' was chosen so that the captured variance divided by the total variance of the mode shapes is greater than 99%, that is,

$$\rho_l = \frac{\sum_{i=1}^{D'} \sigma_m}{\sum_{i=1}^{\tilde{D}} \sigma_m} > 99.0\%. \tag{37}$$

For the first three modes the minimum reduced dimension is $D' = 4$, for the fourth mode $D' = 5$ and for the fifth and sixth mode $D' = 10$.

The clustering algorithm does not take into account an important restriction. Clustering of the modes computed from one specific realization of input parameters should be unique. This uniqueness criterion was implemented after the clustering to check each sample point whether it has two modes classified to the same cluster. In this case, the sample point should be deleted or otherwise adjusted so that all sample points meet the uniqueness criterion.

The clustering worked smoothly for the first three modes with no samples failing in the uniqueness criterion. For mode four, the shapes were only clustered to flipped and not flipped clusters, whereas the shapes from the first one were multiplied by −1. The most problematic was to cluster modes five and six. Here, roughly 1% of the sample points failed the uniqueness criterion and were eliminated from further analysis. The main problem was that some higher mode shapes switched with any of these two modes. Unfortunately, even after filtering sample points by the uniqueness criterion, the clustering fails to give good results for modes five and six. This was observed from the quality of the gPC surrogate model computed by cross-validation (it was also visible when plotting the clustered mode shapes). The second stage filtering for modes 5 and 6 was performed, so that the sample points with the highest errors in the cross-validation process were identified as outliers and filtered out. A similar procedure to 10-fold cross-validation was selected for filtering. 90% of sample points were used to build a surrogate model (gPC with different degrees) and the remaining 10% of sample points were the basis for filtering. In each of 10 folds, 1% of validation sample points with the highest errors were filtered out. By repeating this process with varying degrees of the surrogate (up to the 6th degree), we filtered out roughly 20% of all sample points. The filtering was sufficient for mode 5, but not for mode 6, which still showed too large an error of the surrogate model. Mode 6 was therefore eliminated from further analysis.

From the procedure described above it can be concluded that more degrees of freedom could be included for easier distinguishing between the modes and better clustering results (even though they are not used later for comparison with the experimental results). Even though this would lead to higher dimension D, with the help of the low-rank representation presented in Section 2.3, the increase of the reduced dimension D' would not be significant. Another conclusion is that it would be beneficial to save more modes, to avoid problems when higher modes change order. Another trick might be to include modal mass in the vector used for clustering. This would make it easier to distinguish between the modes, especially between local and global modes, which are often similar given a limited number of degrees of freedom.

Due to the fact that the reference parameters have standard uniform distribution, we used multivariate Legendre polynomials in the expansion, because they are orthogonal with respect to this underlying probability measure. Approximations with polynomials of different degrees were tried and the final degree was chosen by validation. One of the techniques for the validation of the surrogate model is a repeated random sub-sampling validation, where the set of Q sample points is divided randomly between the training set and the validation set.

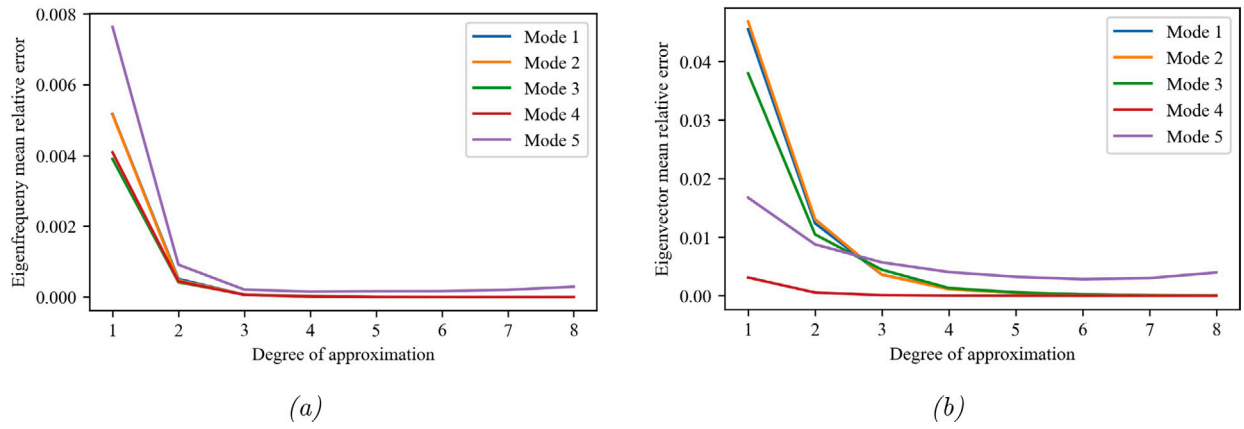

Fig. 8. Cross-validation results for (a) eigenfrequencies and (b) eigenvectors.

85% of the sample points, the training set, are used to fit a surrogate model and the remaining 15% of the sample points, the validation set with V sample points, are used to estimate the error. The procedure is repeated with 10 random splits. The mean relative error of the gPC approximation of the kth eigenfrequency was estimated by

$$\epsilon_{rel,f_k} = \frac{1}{10}\sum_{r=1}^{10}\frac{1}{V}\sum_{j=1}^{V}\frac{|\hat{f}_k^{rt}(\mathbf{p}_{Vr,j}) - f_k(\mathbf{p}_{Vr,j})|}{|f_k(\mathbf{p}_{Vr,j})|}, \tag{38}$$

where f_k denotes the kth eigenfrequency computed by the FE model and $\hat{f}_k^{rt}$ is its gPC approximation of maximum total degree t computed from the training points of the rth split. The $\mathbf{p}_{Vr,j}$ point is the jth validation parameter point of the rth split. This mean relative error of the gPC model for eigenfrequencies is shown in Fig. 8(a). The mean relative error of the surrogate model of the eigenvector $\boldsymbol{\psi}_k$ was computed similarly as

$$\epsilon_{rel,\boldsymbol{\psi}_k} = \frac{1}{10}\sum_{r=1}^{10}\frac{1}{V}\sum_{j=1}^{V}\frac{\|\hat{\boldsymbol{\psi}}_k^{rt}(\mathbf{p}_{Vr,j}) - \boldsymbol{\psi}_k(\mathbf{p}_{Vr,j})\|_2}{\|\boldsymbol{\psi}_k(\mathbf{p}_{Vr,j})\|_2}. \tag{39}$$

The computed relative errors are shown in Fig. 8(b). Based on the results of the cross-validation, a gPC expansion with maximum total degree 4 is chosen for the eigenfrequencies (where all mean relative errors are below 0.0003) and a maximum total degree 6 is chosen for the eigenvectors (where all mean relative errors are below 0.003). Once the surrogate model is determined, it produces modes not in the order of the frequencies but in a predefined order corresponding to the numbering of the different identified clusters that are also matched with the suitable experimental mode shapes.

3.3. Sensitivity analysis and uncertainty quantification

With a surrogate model at hand, several stochastic analyses can be performed relatively quickly. The analyses carried out are uncertainty quantification and sensitivity analysis, presented in this section, and Bayesian inference in Section 3.5.

To estimate the uncertainty of the model, one can perform uncertainty quantification by analysing the probability distributions of the quantities of interest (in our case eigenfrequencies and eigenvectors). The mean value and the variance of the outputs can be calculated using Eqs. (27) and (28). In this way, it is possible to evaluate the confidence in the model based on the prior knowledge about the uncertainty of the input parameters. Moreover, the uncertainty of the model can also be estimated after the Bayesian update is complete using the posterior distribution of the input parameters. The posterior can be determined very efficiently by Monte Carlo sampling due to computationally inexpensive surrogate model. The results are presented in Section 3.6

Global sensitivity analysis can also be performed inexpensively to find the influence of varying the input parameters (individually or in combination) on the variance of the quantity of interest. The Sobol indices are normally computed by Monte Carlo simulation, but with the available gPC surrogate model they can be computed analytically [33]. The Sobol sensitivity indices of the eigenfrequencies and the eigenvectors are shown in Fig. 9. From the results it can be observed that parameters e_1, g_1 and q are the most influential parameters for modes 1 to 3. Other parameters (also higher-order interaction between the parameters) turn out to be more important for modes 4 and 5. Parameter g_2 stands out as the most influential for mode 5. From Fig. 9 it can also be observed that the components of the eigenvectors may be affected differently by varying the different parameters (e.g. components 1 to 13 of mode 4 are not influenced by parameter g_1, whereas components 14–26 are).

3.4. Experimental modal testing

The testing of the building was performed by three synchronized shakers with a total moving mass of 68.85 kg. Altogether 26 accelerometers were installed at 13 sensor locations: 2 sensor locations on each floor (no sensors were placed on the ground floor) and an additional one on the 6th floor, with reference sensors near the shakers. Each sensor location measured accelerations in two horizontal directions, x_1 and x_2, as shown in Fig. 10. Due to the restricted access, the sensors were placed only on the corridors. This provided limited information about the motion of the building and resulted in spatial aliasing. Two sets of 30 min random vibration tests were carried out, one with shakers exciting in the x_1 direction and the other in the x_2 direction. The measured response was divided into 22 windows of 80 s, from which FRFs were obtained. A single-input multiple-output modal identification method, called complex mode indicator function (CMIF), was used on averaged FRF to get eight eigenfrequencies. The first five are shown in Table 2; see also point 4 in Fig. 3 for an illustration of the procedure. For a description of experimental eigenvectors, we refer to [36], where more details on testing are available.

The comparison of two eigenvectors is often performed with MAC measure of correlation, see [39], which handles both real and complex eigenvectors:

$$\mathrm{MAC}(\boldsymbol{\psi}_{k,exp}, \boldsymbol{\psi}_{h,num}) = \frac{\left|\boldsymbol{\psi}_{k,exp}^T \boldsymbol{\psi}_{h,num}^*\right|^2}{\left(\boldsymbol{\psi}_{k,exp}^T \boldsymbol{\psi}_{k,exp}^*\right)\left(\boldsymbol{\psi}_{h,num}^T \boldsymbol{\psi}_{h,num}^*\right)}. \tag{40}$$

Here, $\boldsymbol{\psi}_{k,exp}$ and $\boldsymbol{\psi}_{h,num}$ are the kth experimental and the hth numerical eigenvectors, respectively, and $*$ denotes the conjugation of complex eigenvector. A MAC value of 1 indicates a strong similarity between the two eigenvectors, whereas a value of 0 indicates no similarity. Commonly, a pairwise comparison of the experimental and numerical

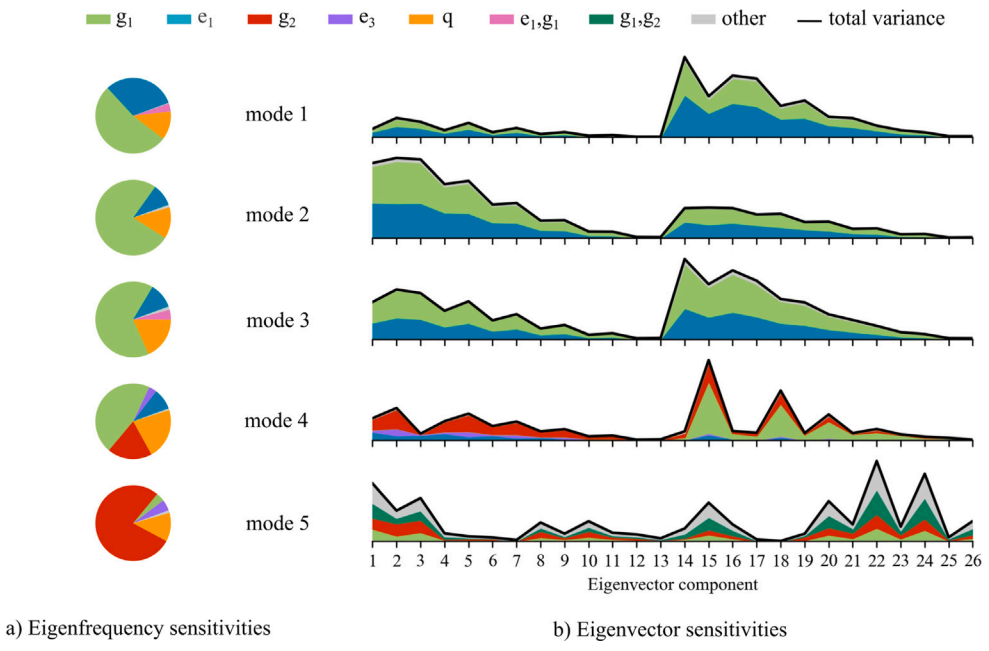

Fig. 9. Sensitivity analysis of the (a) eigenfrequencies and (b) eigenvectors.

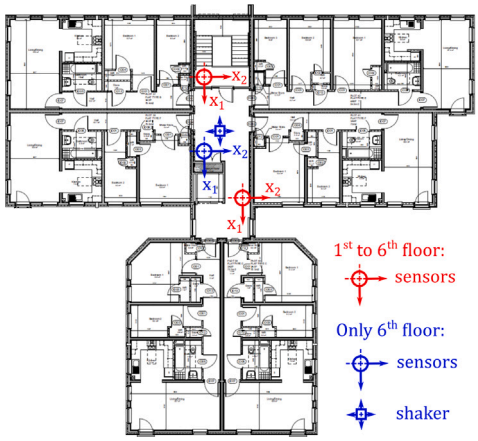

Fig. 10. Layout of shakers and sensors; x_1 and x_2 coordinates.

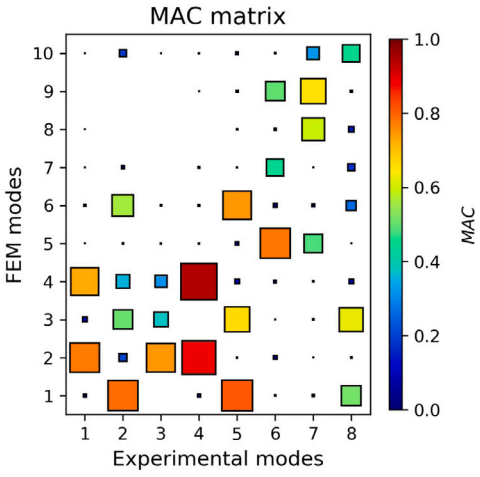

Fig. 11. MAC matrix comparing measured and computed mode shapes (by using mean parameter values).

mode shapes is presented in the MAC matrix. From Fig. 11 it is evident that the MAC matrix for the considered case study suggests a correlation between too many mode shape pairs. This effect is called spatial aliasing and is further discussed in [36]. Due to the ambiguous choice of matching mode pair, the MAC criterion alone is not adequate to be used for pairing numerical modes with the experimental ones.

3.5. Likelihood definition and Bayesian inversion

For model updating in the Bayesian framework, an estimate of the error term in Eq. (4) is needed. The uncertainties of the measured values of the frequencies and the mode shapes (due to the measurement noise and plausible errors made when computing the frequencies and mode shapes from the measured signals) need to be described in the form of a distribution $\pi_{\mathbf{E}}$. We assumed that all modelling errors in the computation of the modal properties by the operator $\mathcal{M}$ are already accounted for in the form of the selected uncertain parameters and we ignored further forms of modelling errors. As a rough estimation, a Gaussian error distribution was assumed

$$\mathbf{E} \sim \mathcal{N}(\mathbf{0}, \boldsymbol{\Sigma}), \tag{41}$$

where the components of the error terms were presumed as independent from each other. Thus, the covariance matrix of the error term $\mathbf{E}$ is diagonal with elements $[\boldsymbol{\Sigma}]_{ll} = \sigma^2_{\mathbf{E},l}$. The standard deviations $\sigma_{\mathbf{E},l}$ for the frequencies were computed from the above-mentioned 22 windows of 80 s and were transformed to FRFs for all 26 degrees of freedom. The samples of the eigenfrequencies were obtained by the peak picking method from a total of 1144 FRFs, see point 4 in Fig. 3 for illustration. The standard deviation of the samples was taken as the standard deviation of the measurement error, see Table 2. The same procedure could not be reliably applied to the eigenvectors. Thus, the standard deviation of the corresponding error components was assumed to be 0.05 based on an educated guess.

Likelihood function $\mathcal{L}(\mathbf{p})$ includes the differences between the FE and experimental frequencies and eigenvectors, see (10). In order to simplify the comparison between complex experimental $\overline{\boldsymbol{\psi}}_{\text{exp}}$ and real FE eigenvectors $\boldsymbol{\psi}_{\text{num}}$, the transformation of the complex experimental eigenvectors to real is performed. The procedure is called realization or real-normalization of mode shapes. How far away a complex

eigenvector is from a real one is characterized by the quantity often named complexity [40], but sometimes also spatiality [41]. The cited literature also provides measures of this quantity. Generally, the higher the complexity, the more error is expected from the process of realization. The complexity of the eigenvector is often associated with the distribution of damping over the structure (highly non-proportional damping corresponds to higher complexity), but this is far from being the only effect. Closely spaced or double modes also contribute to higher complexity as well as analysis and measurement errors. The most common method of getting a real eigenvector is to simply take the modulus of each component of a complex eigenvector and multiply it by the sign of the real part of the component [42]. This works well for low complexity structures with phase angles around 0° or 180°. Another method, presented in [43], may be more widely used. It maximizes the MAC correlation between the original complex vector and the converted real vector. It turns out that this translates to a problem of finding an angle of rotation $\phi_{\max}$ of eigenvector that maximizes the Euclidean norm of the real part of the vector, i.e. $\max \| Re(\overline{\boldsymbol{\psi}}_k e^{i\phi}) \|_2$. The realized eigenvector is then computed as:

$$\boldsymbol{\psi}_k = \frac{Re(\overline{\boldsymbol{\psi}}_k e^{i\phi_{\max}})}{\| Re(\overline{\boldsymbol{\psi}}_k e^{i\phi_{\max}}) \|_2} \tag{42}$$

We used this approach for the realization of the experimental eigenvectors $\boldsymbol{\psi}_k$ that were then used in vector $\mathbf{z}_{\text{meas}}$.

Following Eq. (10) and the multivariate normal distribution, the likelihood in the Bayesian formula reads

$$\mathcal{L}(\mathbf{p}) \approx 2\pi^{-\left(\frac{L}{2}\right)} \det(\boldsymbol{\Sigma})^{-\frac{1}{2}} e^{-\frac{1}{2}(\mathbf{z}_{\text{meas}} - \mathcal{M}_{\text{gPC}}(\mathbf{p}))^T \boldsymbol{\Sigma}^{-1} (\mathbf{z}_{\text{meas}} - \mathcal{M}_{\text{gPC}}(\mathbf{p}))}. \tag{43}$$

It should be noted that in the presented case study forced vibration tests were used as a basis for likelihood, but the herein proposed procedure is not limited to this experimental method. For instance, frequently used AVTs can be applied in this method. However, it is important to note that the estimation of the error term reflects the uncertainty of the experimental eigenfrequencies and mode shapes, which depends on the used measurement procedures (from applied method, execution to the modal identification procedure).

The main objective of the Bayesian inversion is to obtain posterior distribution given in (5)

$$\pi_{\mathbf{P}|\mathbf{z}_{\text{meas}}}(\mathbf{p}) = \frac{\mathcal{L}(\mathbf{p})\pi_{\mathbf{P}}(\mathbf{p})}{\zeta},$$

which can be achieved by sampling from it with the help of the Metropolis–Hastings random walk algorithm described in Section 2.1.

For the proposal density, we used a multivariate normal distribution centred in the current standing point with a diagonal covariance matrix whose diagonal elements we chose to be 0.2% of the prior variances of uncertain parameters $\mathbf{P}$".

For a faster convergence, 100 simultaneous random walks were initiated. A burn-in period of 1000 steps for each random walk was sufficient and then further 10,000 steps were used for evaluation. A total 1,000,000 sample points were acquired and further analysed. Their distribution is shown in Fig. 12. Mean values, standard deviations and the MAP estimate of the posterior parameter distributions are listed in Table 3. Parameters e_1, g_1 and g_2 narrowed their distribution considerably in comparison to the prior, parameters e_3 and q narrowed as well but not as much, whereas parameter e_2 hardly changed its distribution. The standard deviation of the posterior distribution is an indicator of the confidence we have in the updated parameter values, though they should not be taken as exact. From the presented results it is clear that parameter e_2 cannot be identified by the available measurements of the modal properties. The lack of identifiability could already be observed in the sensitivity analysis (see Fig. 9), as none of the used measurements (first five frequencies and mode shapes) were sensitive to this parameter.

Table 2
Uncertainty quantification of eigenfrequencies using prior and posterior parameter distributions together with the estimated mean and standard deviation of the experimental eigenfrequencies.

Mode	Prior		Posterior		Experimental	
	Mean	st. deviation	Mean	st. deviation	Mean	st. deviation
1	2.774 Hz	0.180 Hz	2.842 Hz	0.013 Hz	2.85 Hz	0.024 Hz
2	2.850 Hz	0.192 Hz	2.953 Hz	0.012 Hz	2.93 Hz	0.023 Hz
3	2.937 Hz	0.200 Hz	3.083 Hz	0.013 Hz	3.13 Hz	0.022 Hz
4	3.772 Hz	0.209 Hz	3.741 Hz	0.023 Hz	3.63 Hz	0.043 Hz
5	7.276 Hz	0.555 Hz	6.621 Hz	0.101 Hz	6.73 Hz	0.192 Hz

Table 3
Statistics of the posterior distribution.

Parameter	Mean	Standard deviation	MAP estimate
e_1 [GPa]	6.24	0.23	6.02
e_2 [GPa]	11.68	0.84	12.67
e_3 [GPa]	7.30	1.22	6.14
g_1 [MPa]	734.1	14.2	748.5
g_2 [MPa]	216.8	13.7	201.9
q [kg/m^2]	30.78	9.82	29.98

3.6. Discussion

Analysing the results, we should keep in mind the assumptions we made for the prior and the likelihood. The bounds of the uniform prior parameter distribution reflect the knowledge about material properties, but also take into account any potential modelling error effects that were identified prior to model updating. The second assumption that needs to be considered was the choice of the error function used in the definition of the likelihood function. It should be noted that the posterior strongly depends on the probability description of the parameters and the error term. The magnitude of the assigned uncertainties reflects the engineer's degree of belief and an estimation of the lack of knowledge, as well as an educated guess based on a comprehensive examination of the experimental data and the model. In this way we get an updated stochastic FE model that incorporates all our known formal and informal knowledge about the system, which is unique in terms of the structural details and solutions that are specific to this building. Quantitative results should therefore not be generalized to other buildings, but rather used for qualitative assessment of modelling techniques and the associated model errors.

The results in Fig. 12 are compared with those from deterministic model updating analysed in [36]. It is conclusive from both analyses that there are effects that decrease the vertical stiffness of the walls (i.e. parameter e_1), effects that increase the shear stiffness of the walls (i.e. parameter g_1) and effects that decrease the shear stiffness of the floor slabs (i.e. parameter g_2). However, the current analysis gives additional confidence in the solution at hand. The posterior distribution of those parameters suggests that the mentioned effects are strong, whereas the effects described by parameters e_2 and e_3 are not significant. Furthermore, from the correlation between parameters e_3 and g_2 it can be observed that low values of parameter e_3 might only compensate for the effect captured by parameter g_2. The correlation between parameters e_1, g_1 and g_2 is also informative. Finally, q as a control mass parameter, by being within the reasonable bounds, confirms that it does not compensate for unreasonable stiffness parameters. For further discussion about the effects that are captured within the parameters see [36].

Another added value of the presented approach to model updating with the surrogate model is the possibility to perform uncertainty quantification before and after the update. From Fig. 13 it can be observed that uncertainty decreased significantly after the update for both (a) eigenfrequencies and (b) eigenvectors. Eigenfrequencies that

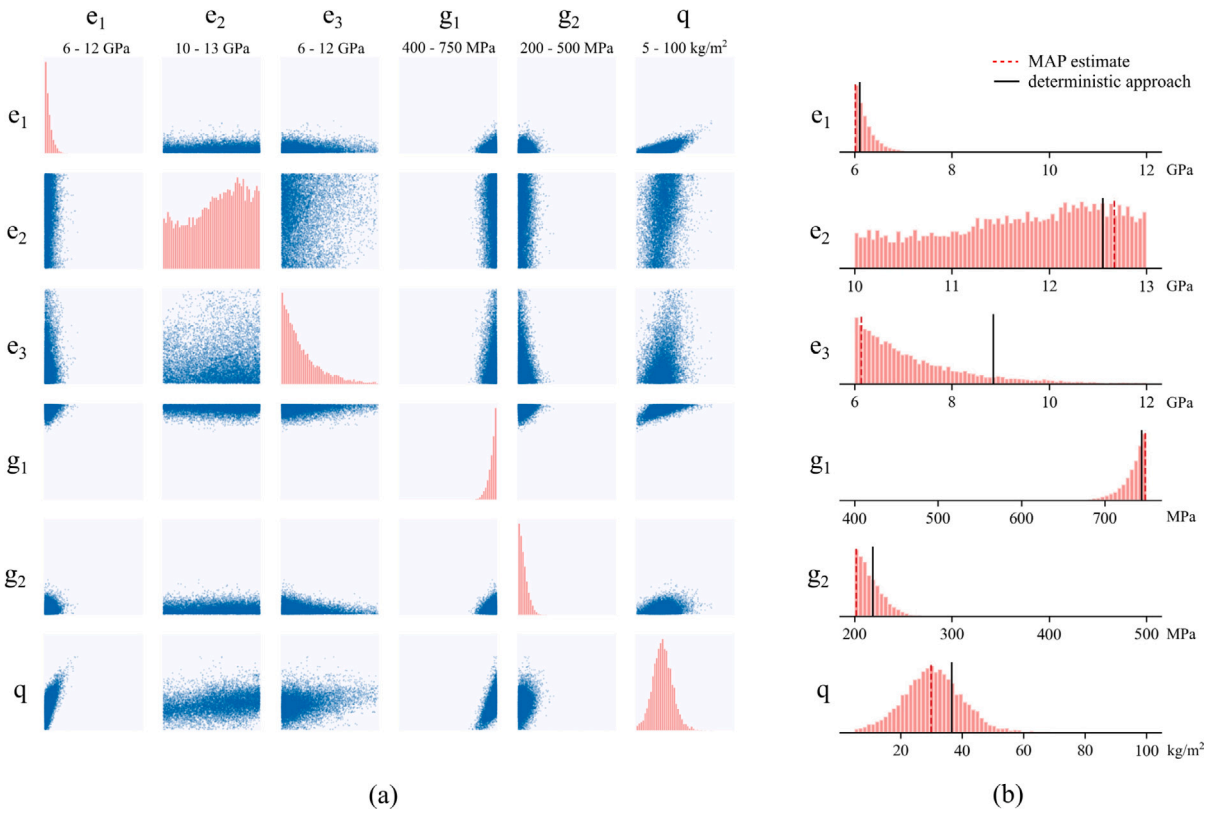

Fig. 12. Samples, drawn from posterior distribution presented in (a) pairwise scatter plot matrix and (b) histograms for all 6 parameters. MAP estimates are compared with the updated values obtained by the deterministic approach.

were predicted prior to the update overlapped considerably, see Fig. 7, but are now easily distinguishable. Fig. 14 shows a relative error between updated eigenfrequencies and experimental ones. Considering the posterior distribution of eigenfrequencies it may be estimated that the relative error for all five eigenfrequencies is below 6%. Results of this study are compared with those from deterministic update [36], where only point estimates are obtained and no confidence interval can be estimated. It can be observed that the estimated eigenfrequencies from deterministic update fall within the range of posterior distribution of eigenfrequencies obtained by the probabilistic approach.

Clear advantages of the probabilistic approach would not be possible without the surrogate model due to the long computation time of the FE model. Difficulties with eigenmode ordering were successfully overcome using the k-means clustering and outlier filtering. The presented approach is particularly useful in cases where MAC proves to be insufficient, i.e. when a high level of spatial aliasing is present or large parameter space is considered.

4. Conclusion and outlook

We applied gPC-based Bayesian model updating on a seven-storey timber (CLT) building. The inference was done by updating six selected model parameters (material and mass properties), chosen to account for a modelling error due to reduced stiffness in the connections and joints between the CLT panels. The quantities of interest are 5 eigenmodes (natural frequencies and mode shapes) measured with the help of a forced vibration test. These measurements were used for the updating of the FE model.

This is an extension of the work presented in [36], where the updating was done by a deterministic approach. The herein presented stochastic approach takes into account not only the expected value of the measured modal properties but also our prior knowledge about the possible values of the input parameters as well as the uncertainties of the measured model properties. Moreover, the procedure not only delivers local minima that yield an FE model providing a good match to the experimental output, but it yields a stochastic FE model that also represents our posterior uncertainties that we have after measuring the modal properties.

To increase the efficiency of the update procedure, a surrogate model is constructed for both eigenfrequencies and eigenvectors. We propose a novel algorithm to handle the problem of eigenmode switching that occurs due to changing of the input parameter values. This problem must be addressed before the computation of the surrogate model. We introduce a low-rank representation of the mode shapes and a machine learning clustering tool (k-means clustering) enhanced with additional outlier filtering. Treating the problem with only the MAC value could not track the mode switching well for this specific application and would result in a faulty non-smooth behaviour of the modal properties, leading to an inaccurate surrogate model. The given procedure can be further improved by including more DOFs (storing a higher resolution of the eigenmodes computed by the FE model, and not only the values at the sensor locations) to improve the efficiency of the clustering method. Facing the curse of dimensionality due to the increment of resolution can be handled by the proposed dimension reduction method of the modal properties. We concluded from the analysis that it is beneficial to store not only the modes intended to be used in the analysis but also higher modes in a preliminary analysis to ensure an efficient mode tracking algorithm.

The surrogate model was used to perform uncertainty quantification, the Sobol sensitivity analysis and finally to carry out the Bayesian update using experimental modal properties. An error term accounting for experimental and modelling errors was estimated based on the variance of eigenfrequencies throughout the duration of the modal testing and engineering expertise. A more accurate estimation of the error of the mode shapes could be achieved by increasing the duration of the vibration tests.

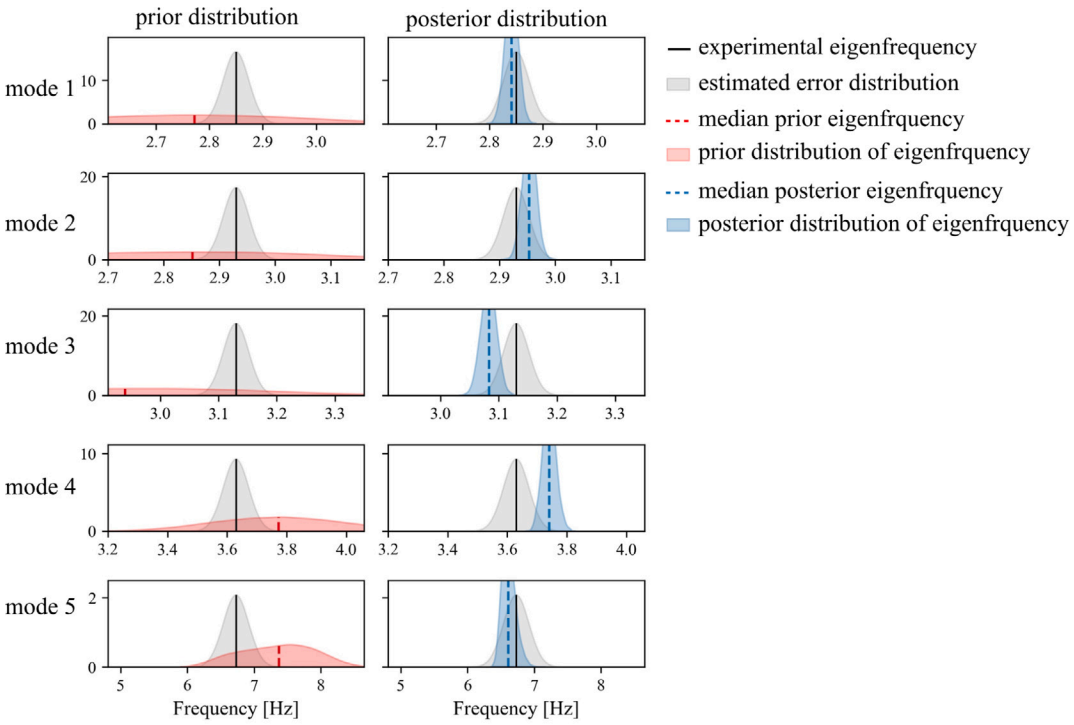

(a)

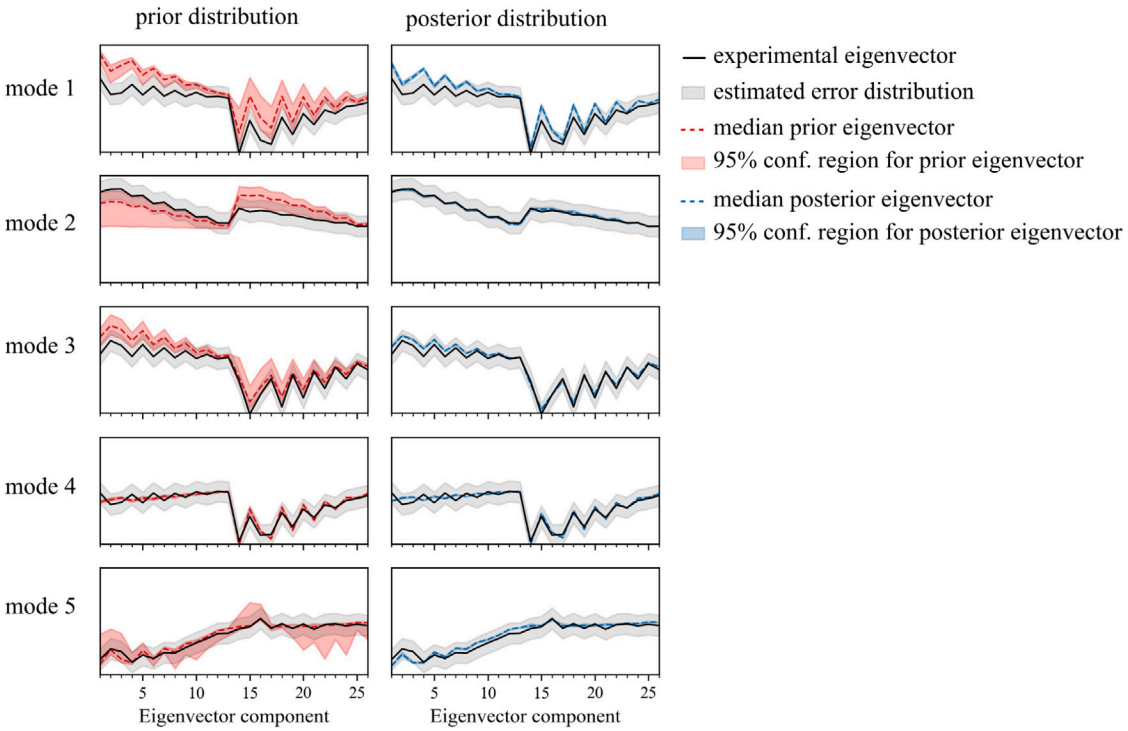

(b)

Fig. 13. Uncertainty quantification of (a) eigenfrequencies and (b) eigenvectors.

CRediT authorship contribution statement

Blaž Kurent: Software, Validation, Investigation, Writing – original draft. **Noemi Friedman:** Methodology, Formal analysis, Investigation, Writing – review & editing. **Wai Kei Ao:** Investigation, Data curation. **Boštjan Brank:** Conceptualization, Supervision.

Declaration of competing interest

The authors declare that they have no known competing financial interests or personal relationships that could have appeared to influence the work reported in this paper.

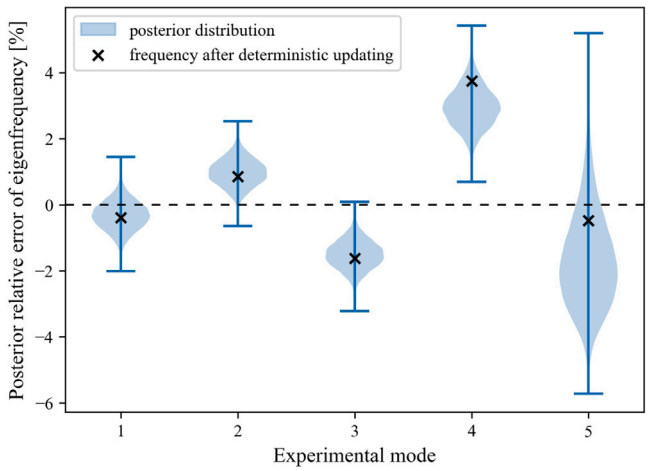

Fig. 14. Comparison of posterior eigenfrequency distribution with experimental point estimates.

Acknowledgements

The support of ERA-NET Cofund Forest Value and the corresponding funding bodies (Ministry of Education, Science and Sport of the Republic of Slovenia for BK and BB, and Forestry Commission GB for WKA) is gratefully acknowledged (DynaTTB project). BK and BB also acknowledge the financial support of the Slovenian Research Agency (J2-2490). The partial support of the Hungarian Ministry of Innovation and Technology NRDI Office within the framework of the Artificial Intelligence National Laboratory Program and the Hungarian National Research, Development and Innovation Office (SNN 134368) is also acknowledged.

References

[1] Necati Çatbaş F, Kijewski-Correa T, Emin Aktan A, editors. Structural identification of constructed systems approaches, methods, and technologies for effective practice of st-id. Reston: American Society of Civil Engineers; 2013.

[2] Mottershead John E, Link Michael, Friswell Michael I. The sensitivity method in finite element model updating: A tutorial. Mech Syst Signal Process 2011;25:2275–96.

[3] Sehgal S, Kumar H. Structural dynamic model updating techniques: A state of the art review. Arch Computat Methods Eng 2016;23:515—533.

[4] Svendsen BT, Petersen ØW, Frøseth GT, Rønnquist A. Improved finite element model updating of a full-scale steel bridge using sensitivity analysis. Struct Infrastruct Eng 2021;1–17.

[5] Naranjo-Pérez J, Jiménez-Alonso JF, Pavic A, Sáez A. Finite-element-model updating of civil engineering structures using a hybrid UKF-HS algorithm. Struct Infrastruct Eng 2021;17(5):620–37.

[6] Yuen K-V. Bayesian methods for structural dynamics and civil engineering. Singapore: John Wiley 'I&' Sons (Asia); 2010.

[7] Jensen H, Papadimitriou C. In: Sub-structure coupling for dynamic analysis. Lecture notes in applied and computational mechanics, vol. 89, Cham: Springer; 2019, p. 179–227, chapter Bayesian Finite Element Model Updating.

[8] Matthies HG, Zander E, Rosić BV, Litvinenko A, Pajonk O. In: Computational methods for solids and fluids. Computational methods in applied sciences, vol. 41, Cham: Springer; 2016, p. 245–86, chapter Inverse Problems in a Bayesian Setting.

[9] Marsili F, Croce P, Friedman N, Formichi P, Landi F. Seismic reliability assessment of a concrete water tank based on the Bayesian updating of the finite element model. ASCE-ASME J Risk Uncertian Eng Syst B 2017;3(2).

[10] Sarfaraz MS, Rosić BV, Matthies HG, Ibrahimbegović A. Bayesian stochastic multi-scale analysis via energy considerations. Adv Model Simul Eng Sci 2020;7:50.

[11] Landi F, Marsili F, Friedman N, Croce P. gPCE-based stochastic inverse methods: A benchmark study from a civil engineer's perspective. Infrastructures 2021;6(11).

[12] Ao WK, Pavic A. FRF-based modal testing of horizontally swaying structures using OCXO synchronised wireless accelerameters for simultaneous force and vibration response measurements. In: Proceedings of the international conference on structural dynamic, EURODYN, Vol. 2. 2020, p. 3301–12.

[13] Pepi Chiara, Gioffre' Massimiliano, Grigoriu Mircea D. Parameters identification of cable stayed footbridges using Bayesian inference. Meccanica 2019;54:1403–19.

[14] Pepi Chiara, Gioffre' Massimiliano, Grigoriu Mircea D, Matthies Hermann G. Bayesian updating of cable stayed footbridbe model parameters using dynamic measurements. In: Eccomas proceedia UNCECOMP. 2019, p. 330–42.

[15] De Falco A, Girardi M, Pellegrini D, Robol L, Sevieri G. Model parameter estimation using Bayesian and deterministic approaches: the case study of the Maddalena Bridge. Procedia Struct Integr 2018;11:210–7.

[16] Behmanesh I, Yousefianmoghadam S, Nozari A, Moaveni B, Stavridis A. Uncertainty quantification and propagation in dynamic models using ambient vibration measurements, application to a 10-story building. Mech Syst Signal Process 2018;107:502–14.

[17] Argyris Costas, Papadimitriou Costas, Panetsos Panagiotis, Tsopelas Panagiotis. Bayesian model-updating using features of modal data : Application to the metsovo bridge. J Sensor Actuator Netw 2020;9(27).

[18] Fotsch D, Ewins DJ. Further applications of the FMAC. In: Proceedings of the international modal analysis conference - IMAC, Vol. 1. 2001, p. 635–9.

[19] Yaghoubi Vahidand, Abrahamsson Thomas. The modal observability correlation as a modal correlation metric. In: Topics in modal analysis, Vol. 7. New York, NY: Springer; 2014, p. 487–94.

[20] Yuen K-V, Beck JL, Katafygiotis LS. Efficient model updating and health monitoring methodology using incomplete modal data without mode matching. Struct Control Health Monit 2006;13:91—107.

[21] Bansal S. Bayesian model updating using modal data based on dynamic condensation. J Eng Mech 2020;146(2):04019123.

[22] Abrahamsen Rune, Bjertnæs Magne A, Bouillot Jacques, Brank Bostjan, Cabaton Lionel, Crocetti Roberto, Flamand Olivier, Garains Fabien, Gavric Igor, Germain Olivier, Hahusseau Ludwig, Hameury Stephane, Johansson Marie, Johansson Thomas, Ao Wai Kei, Kurent Blaž, Landel Pierre, Linderholt Andreas, Malo Kjell, Manthey Manuel, Nåvik Petter, Pavic Alex, Perez Fernando, Rönnquist Anders, Stamatopoulos Haris, Sustersic Iztok, Tulebekova Salue. Dynamic response of tall timber buildings under service load - The DynaTTB research program. In: Proceedings of the international conference on structural dynamic, EURODYN, Vol. 2 (14). 2020, p. 4900–10.

[23] Manthey M, Flamand O, Jalil A, Pavic A, Ao WK. Effect of non-structural components on natural frequency and damping of tall timber building under wind loading. In: World conference on timber engineering 2021, WCTE 2021. 2021.

[24] Mugabo Ignace, Barbosa Andre R, Riggio Mariapaola. Dynamic characterization and vibration analysis of a four-story mass timber building. Front Built Environ 2019;5(July):86.

[25] Aloisio Angelo, Pasca Dag, Tomasi Roberto, Fragiacomo Massimo. Dynamic identification and model updating of an eight-storey CLT building. Eng Struct 2020;213(March):110593.

[26] Reynolds T, Casagrande D, Tomasi R. Comparison of multi–storey cross–laminated timber and timber frame buildings by in situ modal analysis. Constr Build Mater 2016;102:1009–17.

[27] Reynolds Thomas, Harris Richard, Chang Wen Shao, Bregulla Julie, Bawcombe Jonathan. Ambient vibration tests of a cross-laminated timber building. Proc Inst Civ Eng: Constr Mater 2015;168(3):121–31.

[28] Lloyd SP. Least squares quantization in PCM. IEEE Trans Inform Theory 1982;28(2):129–37.

[29] Xiu Dongbin. Numerical methods for stochastic computations: A spectral method approach. Princeton University Press; 2010.

[30] Wiener Norbert. The homogeneous chaos. Amer J Math 1938;60(4):897–936.

[31] Xiu D, Em Karniadakis G. The Wiener-Askey polynomial chaos for stochastic differential equations. SIAM J Sci Comput 2002;24(2):619–44.

[32] Hastings WK. Monte Carlo sampling methods using Markov chains and their applications. Biometrika 1970;57(1):97–109.

[33] Sudret Bruno. Global sensitivity analysis using polynomial chaos expansions. Reliab Eng Syst Saf 2008;93(7):964–79.

[34] Robert Christian P, Casella George. Introducing Monte Carlo methods with R, Vol. 18. Springer, New York, NY; 2010.

[35] Friedman Noémi, Zoccarato Claudia, Zander Elmar, Matthies Hermann G. A worked-out example of surrogate-based Bayesian parameter and field identification methods. In: Bayesian inverse problems. CRC Press; 2021, p. 155–203.

[36] Kurent Blaž, Brank Boštjan, Ao Wai Kei. Model updating of seven-storey cross-laminated timber building designed on frequency-response-functions-based modal testing. Struct Infrastruct Eng 2021;1–19.
[37] Ansys®. Ansys academic research mechanical. 2020, Release 2020 R1.
[38] Enso Stora. European technical assesment ETA-14/0349 of 03.06.2019. Technical report, Austrian institute of construction engineering; 2019.
[39] Allemang RJ. The modal assurance criterion – Twenty years of use and abuse. Sound Vib 2003;37(8):14–21.
[40] Imregun M, Ewins D J. Complex modes-origins and limits. In: Proceedings of the 13th international modal analysis conference. 1995, p. 496–506.
[41] Kozánek Jan. The qualification number of a complex vector. Mech Mach Theory 1987;22(4):391–2.
[42] Friswell Michael I, Mottershead John E. Finite element model updating in structural dynamic. Kluwer Academic Publishers; 1995.
[43] Ahmadian H, Gladwell GML, Ismail F. Extracting real modes from complex measured modes. In: Proceedings of the 13th international modal analysis conference. 1995, p. 507–10.